PAPER

Vortex patterns in rotating dipolar Bose–Einstein condensate mixtures with squared optical lattices

To cite this article: Ramavarmaraja Kishor Kumar *et al* 2019 *J. Phys. B: At. Mol. Opt. Phys.* **52** 025302

IOP Publishing Journal of Physics B: Atomic, Molecular and Optical Physics
J. Phys. B: At. Mol. Opt. Phys. **52** (2019) 025302 (17pp) https://doi.org/10.1088/1361-6455/aaf332

Vortex patterns in rotating dipolar Bose–Einstein condensate mixtures with squared optical lattices

Ramavarmaraja Kishor Kumar[1], **Lauro Tomio**[2,3] and **Arnaldo Gammal**[1]

[1] Instituto de Física, Universidade de São Paulo, 05508-090 São Paulo, Brazil
[2] Instituto de Física Teórica, Universidade Estadual Paulista, 01140-700 São Paulo, Brazil
[3] Instituto Tecnológico de Aeronáutica, DCTA,12.228-900 São José dos Campos, Brazil

E-mail: tomio@ift.unesp.br

Received 5 September 2018, revised 7 November 2018
Accepted for publication 23 November 2018
Published 14 December 2018

Abstract

Vortex-lattice patterns with transitions from regular to other variety vortex shapes are predicted in rotating binary mixtures of dipolar Bose–Einstein condensates loaded in squared optical lattices (OLs). We focus our investigation on the experimentally accessible dipolar isotopes of dysprosium (^{162,164}Dy), erbium (^{168}Er), chromium (^{52}Cr), and rubidium (^{87}Rb), by considering the binary mixtures (^{164}Dy-^{162}Dy, ^{168}Er-^{164}Dy, ^{164}Dy-^{52}Cr and ^{164}Dy-^{87}Rb), which are confined in strong pancake-shaped traps and loaded in squared two-dimensional (2D) OLs, where we vary the polarization angle of the dipoles, the inter-species contact interactions and the rotation frequency. The ratio between inter- to intra-species contact interaction is used for altering the miscibility properties, with the polarization of the dipolar species used for tuning the dipole–dipole interactions to repulsive or attractive. For enough higher rotation, where the inter- to intra-species scattering length ratio is larger than one, in which a richer variety of vortex-lattice patterns are predicted, including vortex sheets and 2D rotating droplet formations. The patterns can be controlled by changing the OL parameters, as shown for the symmetric ^{164}Dy-^{162}Dy dipolar mixture. For mixtures with stronger differences in the dipole moments, such as ^{164}Dy-^{52}Cr and ^{164}Dy-^{87}Rb, only half the quantum vortices and circular ones have been observed, which will depend on the dipole orientations.

Keywords: Dynamic properties of condensates, Bose–Einstein condensates, vortices, periodic potentials, superfluid flow

(Some figures may appear in colour only in the online journal)

1. Introduction

Bose–Einstein condensate (BEC) systems loaded in optical-lattice (OL) potentials are relevant in the investigation of fundamental problems in condensed matter physics [1], such that different accessible experimental possibilities are of interest and merit further study. For instance, by considering a gas of ultra-cold atoms with repulsive interactions held in a three-dimensional (3D) OL, a quantum phase transition from superfluid to a Mott insulator was observed as the potential depth of the lattice is increased [2]. For a considerably large number of atoms localized in single wells of an OL, the mean-field theory can be more safely applied. When there are only a few numbers of atoms in each lattice, the phase coherence between the condensed atoms in the different lattice sites can be lost with the system undergoing a Mott-insulating phase transition [3]. By exploring the phase coherence of coupled quantum gases in two-dimensional (2D) OLs, the lifetime of the condensate and the dependence of the interference pattern on the lattice configuration have been investigated in [4]. Also, BECs loaded in OLs can be used as testing grounds for strongly correlated condensed matter systems [5]. The phase transition between a superfluid-Mott insulator was observed experimentally in a rubidium ^{87}Rb cold-atom gas [6].

Mixtures of atomic BECs with different species can provide a broader range of possibilities to study quantum phenomena. Since 1997, there have been experimental investigations with two-component mixtures of hyperfine states of ^{87}Rb [7]. Further, different heteronuclear atomic species have been combined to produce BEC mixtures. The mass imbalance between the heteronuclear species and their particular intra- and inter-species interaction and the selective tuning of the intra- and inter-species interaction have allowed the investigation of several interesting phenomena. Recent experimental progress with ^{168}Er and ^{164}Dy condensates, as well as with their mixtures are challenging and stimulating present investigations on the properties of dipolar BECs [8–14]. Experiments reported on the stability and collapse of single-component dipolar BECs loaded in an OL can be found in [15]. Also, single-component dipolar gases in a 2D OL have been studied theoretically by using the Bose–Hubbard model and mean-field approximation, from which new quantum phases are predicted, such as checkerboard or supersolid phases [16, 17].

From experiments reported in [18], vortices pinning in rotating BECs have been observed, in which an orientation locking between the vortices and the OLs was verified. By considering the effects of 2D triangular and squared OLs, it was also shown that a sufficiently high squared OL will induce a structural crossover in the vortex lattice. In [18], it is also explained how vortex nucleations depend on the depth of the OL potential and on the rotation frequency. Later, in [19], the existence of a linear dependence of the number of vortices was demonstrated with respect to the rotation frequency in the case of a deep OL. It is common to observe square vortex lattices in binary mixtures of rotating BECs in a harmonic trap [20, 21]. But, a single BEC loaded in a rotating OL can show a rich variety of vortex structural transitions, including square vortex structures [22–24], when playing with other parameters of the condensed atomic gas. An increasing depth of the OL potential helps to reduce the critical rotation frequency necessary to appear as a single vortex. This potential is considered deep when it is greater than the chemical potential of the system.

Previous studies dealing with vortices in dipolar BECs have explained the role of dipole–dipole interactions (DDIs) in the formation of vortices [25]. In particular, the theoretical analysis dealt with the calculation of the critical rotation frequency and vortex structures under the action of the DDI [26–28]. Two-component dipolar BECs in pancake-type traps have been shown to feature several types of vortex lattices, which can be observed by controlling parameters such as the rotation frequency, the ratio between inter- to intra-species scattering lengths, as well as the magnetic moment orientations of the dipoles. In this regard, by considering an opposite polarized two-component BEC with strong DDI in three dimensions, a dynamical study on stability and pattern formation was recently reported in [29]. In these kinds of studies, the addition of OL potentials is also expected to show some relevant effects in vortex-lattice structures, which are worthy of investigation. In this direction, we notice some recent theoretical simulations in [30], by considering OL effects in BEC with the dipolar atomic elements ^{52}Cr, ^{164}Dy and ^{168}Er. These works, besides being limited to an OL in just one of the directions of the pancake-type harmonic trap, are already indicating that rich structures can be obtained by extending the OL in a symmetric way to the two directions of the 2D trap. It is also of interest to explore the region of parameter space, by varying the inter- to intra-species scattering ratios, which can be performed via Feshbach techniques [31], as well as dipolar parameters by also studying other experimentally accessible dipolar condensed mixtures. For a general approach to computing a vortex lattice in rotating condensed systems with strong repulsive two-body interaction and lattice potentials, we can also point out [32].

Another property that plays a relevant role in dipolar mixtures is the miscibility of two-component BEC systems [33–35]. This property was recently studied by considering the atomic isotopes ^{162,164}Dy and ^{168}Er [36]. With respect to the miscibility of dipolar binary mixtures, the rotational properties differ and show distinct vortex-lattice structures [21]. In view of more recent experiments on tuning the magnetic DDI using a dysprosium condensate, we understand the appeal of investigating the properties of BECs with different coupled dipolar species. In particular, it is appropriate to include dysprosium as one of the coupled species in investigations with dipolar mixtures, in view of its large dipole moment [37].

In the present work, our main interest is to provide a more extended investigation on vortex-lattice structures, focusing on binary dipolar mixtures of cold atoms which are accessible for experimental realization, exploring the possibilities of tuning the DDI under rotating squared OLs. This study is of particular interest in terms of indicating regions of parameters which can be tuned in experimental investigation, as well as in the analysis of density patterns of binary dipolar mixtures, in which some new unusual soliton formations and/or quantum lattice phases can emerge [38]. In addition to the previous binary mixtures that have been studied in [21, 36] (^{164}Dy-^{162}Dy and ^{168}Er-^{164}Dy), here we also discuss two cases of coupled systems that are less symmetric in their DDI as well as in their respective masses, which are ^{164}Dy-^{52}Cr and ^{164}Dy-^{87}Rb. For the mixture with ^{87}Rb, which is an atomic element with quite a weak magnetic dipole, we found it unnecessary to explore in detail, once it was verified that the corresponding relevant results follow from cases such as with ^{52}Cr, where one of the dipole moments is not strong. By analyzing mixtures that are partly and completely immiscible, we show a variety of vortex structures that are controlled by larger inter-species contact interactions. Besides the fact that an increasing depth of the OL potential helps to reduce the critical rotation frequency to produce vortices, in our study we assume this potential is not too deep, as limited by the validity of the mean-field model. Supported by our numerical simulations, we provide phase diagrams indicative of the expected vortex-lattice patterns, in a plane defined by the rotation frequency Ω and the ratio between inter- and intra-species scattering lengths δ for two different orientation angles of the dipoles, such that the DDI can be repulsive or attractive.

In the next section 2, we present the formalism that we consider for the treatment of coupled dipolar condensed mixtures, confined by a pancake-shaped harmonic trap with a rotating OL. In section 3, we present our results for the different kinds of coupled mixtures we are considering, together with details on the numerical approach and corresponding parameters. Finally, in section 4 we summarize the main findings with our conclusions.

2. Binary dipolar condensate under rotation loaded in a squared OL

In our present study of coupled two-species dipolar condensates, our main objective is to investigate a rotating condensate under the effect of a squared OL, which is acting together with a strong pancake-shaped harmonic trap in the system. This matter demands to be theoretically studied in view of recent experimental interests with condensed quantum gases with DDI and rotating magnetic fields [38]. By tuning the alignment angle of the two-dipole species, the DDI interaction can be changed from repulsive to attractive. For the 3D DDI kernels, we assume the relative positions of the two-dipole moments make an angle θ relative to a defined z-direction. With that, by considering the condensate in a pancake geometry defined in the (x, y)–plane, with the relative positions between the dipoles being near 90°, we have mainly a repulsive DDI for a static magnetic field fixed in the z-direction.

For the DDI, we follow the scheme as described in [39, 40], with the polarization of both aligned dipoles being under rotation due to a time-dependent rotating external magnetic field. So, we consider the orientations of both dipoles making an angle φ with respect to the z-axis, such that the DDI is repulsive when $\varphi = 0$, becoming attractive for $\varphi > 54.7°$. As detailed in [40], the tunability of the magnetic dipolar interaction is performed by using time-dependent magnetic fields with dipoles rapidly rotating around the z-axis. The magnetic field is given by the combination of a static part along the z-direction and a fast rotating part in the (x, y)–plane, having a frequency which is chosen such that the atoms are not significantly moving during each period. Under these conditions, once a time averaging of the DDI in a period is performed, the corresponding 3D averaged interaction for the coupled two dipolar species, with the magnetic dipole moments μ_1 and μ_2 given in terms of the Bohr magneton μ_B, can be written as

$$\langle V_{3D}^{(d)}(\mathbf{r}_1 - \mathbf{r}_2)\rangle = \mu_0\mu_1\mu_2 \frac{1 - 3\cos^2\theta}{|\mathbf{r}_1 - \mathbf{r}_2|^3}\left(\frac{3\cos^2\varphi - 1}{2}\right), \tag{1}$$

where μ_0 is the free-space permeability. The factor within parenthesis in (1) is the result of the time-averaging procedure on the dipole orientation around the z-axis. The angle φ provides the effective strength and sign of the interaction, with the magnetic dipoles being completely polarized along the z-direction for $\varphi = 0$ (when $V_{ij}^{(d)} > 0$), with the sign being inverted for $\varphi \geqslant 54.7°$ when the interaction becomes attractive. It is worth noticing in equation (1) that the DDI effect can be canceled out at two specific orientations: when the polarization is such that $\cos^2\varphi = 1/3$, or when the relative position of the two dipoles in relation to the z-axis is such that $\cos^2\theta = 1/3$. However, in our following approach we assume $\theta \sim 90°$, as we consider the binary system in a strongly pancake-shaped format.

One of our present aims is to study the effect of a squared OL potential in dipolar mixtures under rotation. This OL potential is added together with the external 3D harmonic trap, which is confining both atomic species $j = 1, 2$ in a strong pancake-shaped symmetry, given by the trap aspect ratio $\lambda = 50$, such that

$$V(\mathbf{r}) = \frac{1}{2}m_j\omega_j^2(x^2 + y^2 + \lambda^2 z^2) + V_{\rm ol}[\sin^2(kx) + \sin^2(ky)], \tag{2}$$

where m_j and ω_j are, respectively, the mass and trap frequency of the species j. The strength of the OL potential is given by $V_{\rm ol}$, with π/k defining the lattice periodicity which is assumed to be identical in the x and y directions.

The strong pancake-shaped symmetry ($\lambda = 50$) assumed along this study, is considered due to stability requirements. With such strong asymmetry, together with the symmetry of the OL potential and the DDI, the corresponding 3D coupled equation is reduced to a 2D format, by the usual factorization of the 3D wave function $\Psi_j(\mathbf{r}, t)$ into the ground state of the transverse harmonic oscillator trap and a 2D wave function [21, 41–44], with

$$\Psi_j(\mathbf{r}, t) = \left(\frac{\lambda}{\pi l^2}\right)^{1/4} e^{-\lambda z^2/(2l^2)}\, \Phi_j(x, y, t). \tag{3}$$

Next, we perform the 2D reduction by introducing the above ansatz in the original 3D Gross–Pitaevskii (GP) formalism with DDI, integrating over the variable z. The final coupled equations are cast in a dimensionless format by measuring the energy in units of $\hbar\omega_1$, with the length in units of $l \equiv \sqrt{\hbar/(m_1\omega_1)}$. For this purpose, the space and time variables are given in units of l and $1/\omega_1$, respectively, with $\mathbf{r} \to l\mathbf{r}$ and $t \to \tau/\omega_1$. Within this procedure, the corresponding dimensionless wave-function components are given by $\psi_j(x, y, \tau) \equiv l\Phi_j(x, y, t)$. The two-body contact interactions related to the scattering lengths a_{ij}, as well as the DDI parameters for the species $i, j = 1, 2$ are defined as

$$g_{ij} \equiv \sqrt{2\pi\lambda}\frac{(m_1 + m_2)}{m_2}\frac{a_{ij}N_j}{l}, \quad \mathrm{d}_{ij} = \frac{N_i}{4\pi}\frac{\mu_0\mu_i\mu_j}{\hbar\omega_1 l^3},$$
$$a_{ii}^{(d)} \equiv \frac{1}{12\pi}\frac{m_i}{m_1}\frac{\mu_0\mu_i^2}{\hbar\omega_1 l^2}, \quad a_{12}^{(d)} = a_{21}^{(d)} = \frac{1}{12\pi}\frac{\mu_0\mu_1\mu_2}{\hbar\omega_1 l^2}, \tag{4}$$

where $N_{j=1,2}$ is the number of atoms in the species j. With the assumption that both components are confined by pancake-shaped harmonic traps with the same aspect ratio λ and such that the relation between the corresponding trap frequencies is given by $m_2\omega_2^2 \simeq m_1\omega_1^2$, in terms of the above notation for the units and parameters, the corresponding coupled 2D GP

equations (with $i, j = 1, 2$ and $j \neq i$) can be written as

$$\mathrm{i}\frac{\partial \psi_i}{\partial \tau} = \left[-\frac{m_1}{2m_i}\left(\frac{\partial^2}{\partial x^2} + \frac{\partial^2}{\partial y^2}\right) + V(x, y) - \Omega L_z + \sum_{j=1,2} g_{ij}|\psi_j|^2 + \sum_{j=1,2} \mathrm{d}_{ij} \int_{-\infty}^{\infty} \mathrm{d}x'\mathrm{d}y' V_{2D}^{(d)}(x - x', y - y')|\psi_j'|^2 \right]\psi_i, \tag{5}$$

where $V^{(d)}(x, y)$ is the 2D expression for the DDI, which is to be derived from the corresponding 3D counterpart given in equation (1), and $\psi_i \equiv \psi_i(x, y, \tau)$ and $\psi_i' \equiv \psi_i(x', y', \tau)$ are the components of the total 2D wave function, normalized to one, $\int_{-\infty}^{\infty} \mathrm{d}x\mathrm{d}y|\psi_i|^2 = 1$. L_z is the angular momentum operator with Ω the corresponding rotation parameter (in units of ω_1), which is common for two components. In this 2D reduction, the external potential provided by the harmonic trap, together with the squared OL, in dimensionless units is given by

$$V(x, y) = \frac{1}{2}(x^2 + y^2) + V_0[\sin^2(kx) + \sin^2(ky)], \tag{6}$$

where $V_0 \equiv V_{ol}/\hbar\omega_1$ gives the strength of the OL in dimensionless units, with k being the laser wave vector (also dimensionless and being the same in both x and y directions).

The 2D DDI is presented in equation (5) can be expressed by means of the convolution theorem, which is given by the inverse 2D Fourier transform for the product of the DDI and densities, as

$$\int \mathrm{d}x'\mathrm{d}y' V^{(d)}(x - x', y - y')|\psi_j'|^2 = \mathcal{F}_{2D}^{-1}[\widetilde{V}^{(d)}(k_x, k_y)\tilde{n}_j(k_x, k_y)], \tag{7}$$

where $\tilde{n}_j(k_x, k_y)$ is the 2D Fourier transform of the density,

$$\tilde{n}_j(k_x, k_y) = \int \mathrm{d}x\mathrm{d}y\, e^{\mathrm{i}(k_x x + k_y y)}|\psi_j|^2, \tag{8}$$

with $\widetilde{V}^{(d)}(k_x, k_y)$ being the Fourier transform of the DDI, which is expressed by the combination of two terms, corresponding to parallel and perpendicular polarizations of the dipoles in relation to the z-direction [45]:

$$\widetilde{V}^{(d)}(k_x, k_y) \equiv \cos^2(\varphi)\widetilde{V}_{\perp}^{(d)}(k_x, k_y) + \sin^2(\varphi)\widetilde{V}_{\parallel}^{(d)}(k_x, k_y). \tag{9}$$

The DDI is perpendicular when the two dipoles are polarized in the z-direction ($\varphi = 0$),

$$\widetilde{V}_{\perp}^{(d)}(k_x, k_y) = 2 - 3\sqrt{\pi}\left(\frac{k_\rho}{\sqrt{2\lambda}}\right)\exp\left(\frac{k_\rho^2}{2\lambda}\right)\mathrm{erfc}\left(\frac{k_\rho}{\sqrt{2\lambda}}\right), \tag{10}$$

and longitudinal when the dipoles are polarized in the (x, y) plane ($\varphi = 90°$),

$$\tilde{V}_{\parallel}^{(d)}(k_x, k_y) = -1 + 3\sqrt{\pi}\left(\frac{k_\rho \cos^2\theta_k}{\sqrt{2\lambda}}\right) \times \exp\left(\frac{k_\rho^2}{2\lambda}\right)\mathrm{erfc}\left(\frac{k_\rho}{\sqrt{2\lambda}}\right) \tag{11}$$

where $k_\rho \equiv \sqrt{k_x^2 + k_y^2}$, with θ_k being an arbitrary direction in the momentum plane defined by $(k_x, k_y) = (k_\rho \cos\theta_k, k_\rho \sin\theta_k)$. As all θ_k are equally possible, by averaging $\cos^2\theta_k$ we obtain a factor $1/2$. So, the total DDI is averaged to zero for $\varphi = 54.7°$, being repulsive for $\varphi < 54.7°$ and attractive for $\varphi > 54.7°$. As the system trapped in an OL potential can become unstable when the dipolar BEC is tuned to larger angles, the attractive part of the DDI is restricted to $\varphi \leqslant 60°$.

3. Vortex-pattern results: dipolar mixtures in OLs

Our main results are reported in this section, by considering different kinds of coupled dipolar systems. An isotope of the dysprosium was chosen as a common element in the mixtures in view of its large magnetic moment, as well as due to the fact that this element was considered in recent experimental BEC realizations in ultra-cold laboratories. We select a few sample results indicating the rich variety of vortex-lattice patterns, which are obtained with dipolar mixtures under rotation with squared OLs. For the more illustrative cases of symmetric- and asymmetric-dipolar mixtures, we present diagrams considering the rotation parameter as a function of the ratio between inter- to intra-species contact interactions, for repulsive and attractive DDI. These diagrams, which summarize the kind of vortex-lattice patterns that we have obtained, are followed by characteristic examples.

Before reporting the specific dipolar systems we have obtained, next we provide some details on the corresponding physical parameters and numerical approach.

3.1. Parameter space and numerical approach

Of particular relevance to the present study on dipolar binary mixtures is to consider atomic species accessible to experimental realizations in ultra-cold atom laboratories, which have significant magnetic dipole moments. By considering the dipole moments of each species, the corresponding dipolar parameter of the DDI will be fixed for each specific mixture. In this regard, for the binary mixtures we are using, the corresponding magnetic dipole moments given in terms of the Bohr magneton μ_B, are the following: $\mu = 10\mu_B$ for ^{162,164}Dy, $\mu = 7\mu_B$ for ^{168}Er, $\mu = 6\mu_B$ for ^{52}Cr and $\mu = 1\mu_B$ for ^{87}Rb. In particular, considering the corresponding dipole moments, the strengths of the DDI are given as $a_{ij}^{(d)} = 131\, a_0$ $(i,j = 1, 2)$, for the ^{164}Dy-^{162}Dy mixture; $a_{11}^{(d)} = 66\, a_0$, $a_{22}^{(d)} = 131\, a_0$ and $a_{12}^{(d)} = a_{21}^{(d)} = 94\, a_0$, for the ^{168}Er-^{164}Dy mixture; and $a_{11}^{(d)} = 131\, a_0$, $a_{22}^{(d)} = 16\, a_0$ and $a_{12}^{(d)} = a_{21}^{(d)} = 25\, a_0$, for the ^{164}Dy-^{52}Cr mixture. Once the

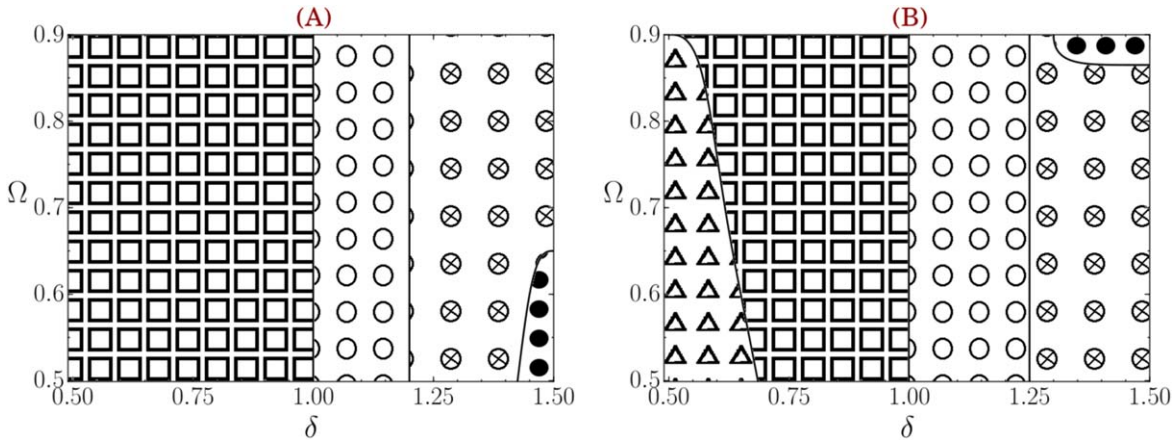

Figure 1. Diagrammatical representations of vortex-lattice patterns obtained for the ^{164}Dy-^{162}Dy dipolar mixture, with the rotation frequency Ω as a function of the contact interaction ratio $\delta \equiv a_{12}/a_{11}$ in a plane defined by Ω (in units of ω_1) and contact interaction ratio $\delta \equiv a_{12}/a_{11}$. Both dipoles are polarized: along the z-axis ($\varphi = 0$) in (A); and at an angle $\varphi = 60°$ in (B). The symbols filling specific intervals indicate the approximate observed vortex-lattice patterns in these regions: squares for squared lattices; triangles for triangular lattices; circles for double-core or striped vortices; crossed circles for domain walls or vortex sheets; and solid circles for 2D rotating droplets.

DDI is fixed, in order to explore various families of vortex patterns we vary the rotation frequency Ω, the polarization angle φ, as well as the ratio δ between inter- and intra-species contact interaction.

Apart from dipolar parameters, other intrinsic properties of binary systems are related to the two-body contact interactions, which in principle can be varied by using Feshbach techniques [31]. In order to keep our study to stable systems, all the two-body scattering lengths are assumed to be positive, with the intra-species ones being identical and given by $a_{11} = a_{22} = 40a_0$ (a_0 is the Bohr radius), with the inter-species one, a_{12}, obtained from the ratio $\delta = a_{12}/a_{11}$. Relevant for the vortex patterns that we are studying, we allow δ to be changed in a region of interest in the parameter space, from smaller to larger values, together with the parameter Ω related to the rotation of the condensate and parameters of the squared OL.

The contact and DDI parameters, which appear in equation (5) as dimensionless (g_{ij} and d_{ij}, respectively) are given in units of the Bohr radius a_0 by (4). By varying these parameters we contemplate several conditions of interest in view of miscibility properties of the binary mixtures (see a previous study in [36] without an OL). For the usual harmonic trap, in all the following simulations and analysis of the results we consider a strong pancake-shaped trap in the (x, y)–plane, with an aspect ratio $\lambda = 50$, fixing the number of atoms for both species as $N_1 = N_2 = 10^4$. These choices are appropriate for experimental realistic settings due to stability requirements. The assumed angular frequencies of the harmonic axial traps are such that $m_2\omega_2^2 \simeq m_1\omega_1^2$, implying that $\omega_j = 2\pi \times 60\ \mathrm{s}^{-1}$ for the ^{168}Er and $\omega_j = 2\pi \times 61\ \mathrm{s}^{-1}$ for the ^{162,164}Dy.

The external trap is modified by the addition of a squared OL, defined in the same (x, y)-plane. By choosing the spacing of the OL given by $d_{lat} = \lambda_L/2 \approx 534$ nm, as in the experiments reported in [46], the corresponding wavelength of the laser is $\lambda_L = 1064$ nm. So, with the time and space units such that $1/\omega_1 = 2.65$ ms and $l = 1$ μm, the corresponding dimensionless parameters for the OL spacing is $\pi/k = 0.534$; or $k = 1.87\pi$. In the results that we are presenting the OL depth was fixed to $V_0 = 15$. However, by investigating other strengths, going up to $V_0 = 25$, we have observed that the vortex structural properties remain essentially unchanged.

In order to solve equation (5), we employ the split-step Crank–Nicolson method, as in [43, 47, 48], combined with a standard method for evaluating DDI integrals in the momentum space [39, 43]. In order to search for stable solutions, the numerical simulations were carried out in imaginary time on a grid with maximum of 640 points in x and y directions, with spatial steps $\Delta x = \Delta y = 0.05$ and time step $\Delta t = 0.000\ 5$. Both component wave functions are renormalized to one at each time step. In order to obtain stationary vortex states, we solve equation (5) with different initial conditions. In view of previous tests on the initial suitable conditions, we use a combination of angular harmonics, followed by verifying the convergence of the solutions for the inputs, as discussed in [21, 49–51].

3.2. Symmetric-dipolar mixture ^{164}Dy-^{162}Dy in a squared OL

Our analysis on dipolar mixtures starts by considering the symmetric case with a coupled dipolar mixture of two dysprosium isotopes, ^{164}Dy and ^{162}Dy, such that the strengths of the DDI are the same, given by $a_{ij}^{(d)} = 131\ a_0$ (i, $j = 1$, 2). The main characteristics of this system, verified in previous studies, is that it is completely miscible as verified in a study without an OL, having the same value close to one for the miscibility parameter defined in [36], implying in an almost complete overlap between the densities of the two components. In view of the miscibility of the two components, the parameter δ, which gives the ratio between the inter- and intra-species scattering length, plays the main role for the observation of quite different vortex patterns, for a given rotation Ω.

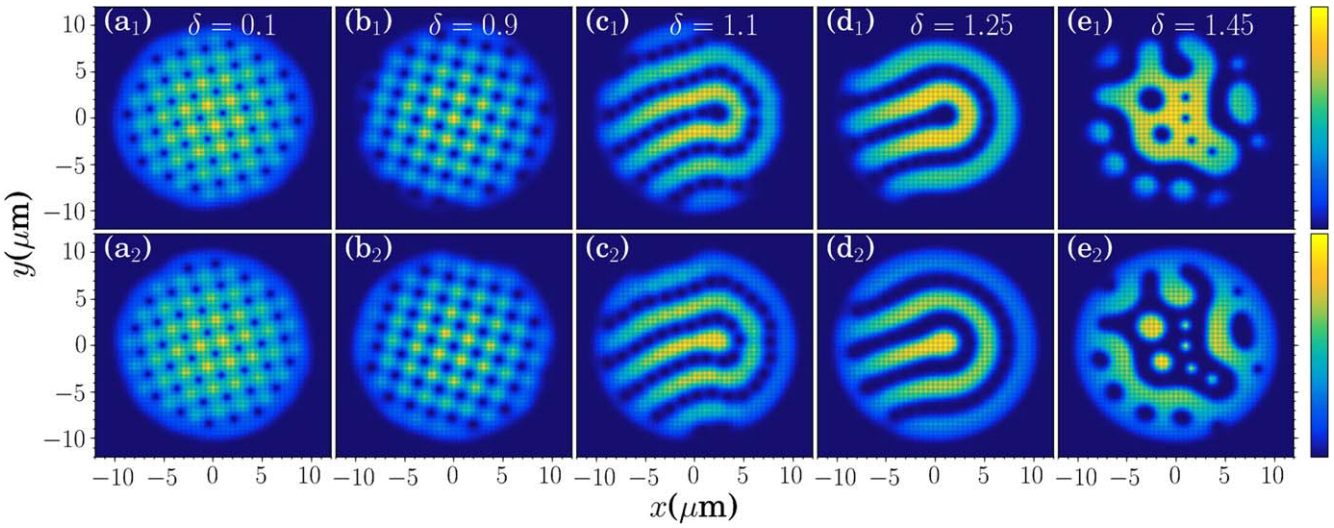

Figure 2. The 2D densities $|\psi_j|^2$ for the symmetric-dipolar mixture ^{164}Dy-^{162}Dy (when $a_{ij}^{(d)} = 131a_0$, $i, j = 1, 2$) are shown in the (x,y) plane for different stable lattice-vortex patterns, with $0.1 < \delta < 1.45$ (as indicated inside the panels), considering $\Omega = 0.5$ (units of ω_1). Both dipole orientations are parallel to the z-axis ($\varphi = 0$, repulsive DDI), with the OL parameters being $V_0 = 15$ ($\hbar\omega_1$ units) and $\pi/k = 0.534$ (μm units). The other parameters are $N_j = 10^4$, $\lambda = 50$, and $a_{jj} = 40a_0$. Starting from zero (darker), the maximum density levels (clearer) are 0.009 for (a_j) and 0.012 for the other panels, in $(\mu\text{m})^{-2}$ units.

In figure 1, by considering our results with different values of Ω (from 0.5 to 0.9) and δ (from 0.5 to 1.5), we present two diagrams which indicate the main characteristic of vortex patterns that are obtained for the ^{164}Dy-^{162}Dy dipolar mixture, confined by a strong pancake-type harmonic trap with a squared OL (having strength $V_0 = 15$). In this figure, we consider two different orientations for the dipoles of the coupled mixture, in relation to the z-axis. In the diagram (A) we have the dipoles oriented parallel to z, such that $\varphi = 0°$ for the corresponding angle. With this orientation the DDI is repulsive. For the results shown in the diagram (B), the dipole polarizations are tuned to an angle $\varphi = 60°$ in relation to the z-axis, supporting an attractive DDI. In both the panels, for a given region (Ω, δ), the kind of observed vortex patterns are being identified by the symbols filling the respective region: (i) with squares, for squared-vortex lattices; (ii) with empty circles, for double-core or striped vortex patterns; (iii) with triangles, for triangular-vortex lattices; (iv) crossed circles, for domain-wall or vortex-sheet patterns; and (v) solid circles, for lattice patterns with quantum rotating droplet formations[4].

As observed for this symmetric mixture, when the dipoles are aligned along the z-axis, for $\delta \leqslant 1$, the OL is changing the lattice patterns from triangular ones, which have been verified when no OL is active, to squared lattice patterns. This kind of pattern has been observed even for $\delta = 0.1$, with the effect of the OL being more evident in the regions where inter-species contact interaction is considerably smaller than intra-species interaction. As shown in the phase diagram (A), for the case that $\varphi = 0$ (when the dipoles are aligned with z), for $1 < \delta \lesssim 1.2$ the patterns change to double-core and striped vortices; and domain walls for $\delta > 1.2$. These pattern results are almost independent of the value of the frequency parameter Ω, which was varied for $0.9 > \Omega > 0.5$. However, among the patterns with domain walls observed for $\delta > 1.4$, we have also verified lattice patterns with rotating droplets, in case that $\Omega < 0.65$.

By tuning the dipoles to an angle $\varphi = 60°$ in relation to the z-axis, we are providing an attractive dipolar interaction. In the binary mixture, repulsive two-body interactions determine the miscibility properties. So, the attractive dipolar interactions are going to make the system more miscible, reducing the effect of the OL, in particular for smaller values of Ω. Consequently, part of the squared-vortex structures observed when $\delta < 0.7$ in the phase diagram (A) (when $\varphi = 0$), will change to triangular ones, as shown in the phase diagram (B) of figure 1. We can also observe that this attractive dipolar interaction is playing a role in the droplet regime when $\delta > 1$, as the attractive interactions increase the critical rotation frequency for a single vortex. So, the reduction in the number of vortices becomes explicit due to the attractive dipolar interaction. As the rotation velocity $\Omega < 0.85$ is not sufficient to produce the droplet regime, the rotating droplets are observed for $\delta > 1.3$ and $\Omega > 0.85$.

Typical examples of pattern results corresponding to diagram (A) of figure 1, for $\Omega = 0.5$ and 0.9, are displayed in the next figures 2 to 4, in which the dipoles are aligned along the z-axis ($\varphi = 0$). In figure 5 we have results for attractive DDI ($\varphi = 60°$) with rotation frequency $\Omega = 0.9$.

3.2.1. ^{164}Dy-^{162}Dy mixture, with repulsive DDI. For the repulsive case, we start in figure 2 to show the corresponding densities of the two components of the coupled dipolar system, by considering the ratio between two-body inter- and intra-species δ scattering lengths

[4] For 'rotating droplets' we meant droplet-like density oscillations, similar as the ones discussed in [52, 53]. In our present study we are not considering quantum fluctuations, such that these droplets cannot be associated to the self-bound droplets reported in [8, 10] for single-component experiments.

changing from 0.1 to 1.45, which are given in five pairs of panels for the coupled elements of the mixture, in the presence of a squared OL (with $V_0 = 15$), for a given rotation frequency $\Omega = 0.5$. The effect of the squared OL in this case that we have repulsive DDI can be verified by comparing the results with previous results performed without an OL, for $\Omega < 0.6$ and $\delta < 0.6$. We noticed that vortex-lattice patterns with triangular formats observed in [21] are modified to squared formats, when adding a squared OL with a grid size given by $k = 1.87\pi$, as exemplified by the panels ($a_{j=1,2}$). Further, irrespective of the values of Ω, for $\delta \leqslant 1$, we have observed only square-shaped vortex structures, as shown in the panels (a_j) and (b_j). However, when δ becomes larger than one, with the inter-species contact interactions becoming dominant, the miscibility of the two components starts to play a more relevant role, resulting in lattice-vortex structures more favorable to immiscible bosonic systems. These results are represented by the panels (c_j), (d_j) and (e_j), for $\delta = 1.1$, 1.25 and 1.45, respectively. The closely located vortices of each species start to join together forming patterns with domain walls separating the species, resulting in vortex sheets or with serpentine shapes. This behavior in pattern transitions can be seen from (b_j) to (c_j), and from (c_j) to (d_j).

Transition to less regular patterns is observed by enhancing the immiscibility of the mixture, further increasing the relation between inter- to intra-species scattering length δ, as indicated by the panels (e_j). The two dipolar species start to become almost separated, but sharing the same region of space as they are symmetric in their dipolar properties with masses slightly different. Therefore, patterns with different shapes can be observed as we increase the value of δ, where 2D rotating droplet formations can emerge. This behavior is characterized by the panels (e_j), in which it is noticed that the more central region is mainly occupied by the more massive species.

3.2.2. Vortex-lattice changes by varying the OL spacing. The OL spacing used along this work, $\pi/k = 0.534$ (corresponding to $k = 1.87\pi$) is motivated by our main purpose to investigate an experimentally accessible region for coupled dipolar systems, as in [46]. However, in order to verify the effect of the spacing grid given by the OL parameter k in the pattern transitions, we include figure 3 by considering a fixed large value of $\delta = 1.45$ (the same as in the panels (e_j) of figure 2), with k varying from zero to 4π; the first implying there is no OL potential, as shown by equation (6); with the second having a grid spacing so small that the net effect is reduced to a constant in the trap. The panels presented in figure 3 are arranged in an array with six columns and four rows, by contemplating the densities together with their corresponding phases. The first and third rows of panels present the densities $|\phi_j|^2$ for the first ($j = 1$) and second ($j = 2$) components of the mixture, respectively; with the second and fourth rows presenting the corresponding phases (for the panels identified in the first and third rows). The values of k ($= 0, 4\pi, 1.87\pi, 1.5\pi, \pi$ and 0.5π) are fixed at each column, being identified in the first row, such that in the first column we have the case without OL potential. Next, in the other panels we consider the squared OL grid starting from a smaller size ($\pi/k = 0.25$) to a larger size ($\pi/k = 2$). In this regime with $\delta = 1.45$, when switching off the OL with $k = 0$, the patterns are dominated by the repulsive dipolar interactions and rotation frequency ($\Omega = 0.5$), with the results, for densities and phases, being shown in the first column of figure 3. By considering very large values of k, such as $k = 4\pi$ (implying in smaller grid sizes) the results have some similarities with the ones obtained for the case without the OL ($k = 0$), indicating that the OL effect is averaged out. However, by increasing the grid of the OL potential, as shown in the panels with columns identified by (d_j) to (f_j), we notice that the role of the OL is more evident when considering intermediate values of k. With the panels (d_j) for $k = 1.5\pi$ to (f_j) for $k = 0.5\pi$, it is observed that the effect of the OL is dominating, resulting in more geometric patterns, whereas near $k = 1.87\pi$ a transition regime is verified, with the formation of 2D rotating droplets in the mixture.

Without the OL and symmetric binary mixtures, rotating droplets have already been observed in [20], with instabilities and pattern formations having been recently studied in [29], by considering oppositely polarized dipoles in a two-component BEC. Here, by applying a shallow squared OL for the rotation given by $\Omega = 0.5$ 2D droplet shaped densities are formed in the particular regime with $\delta > 1.4$, as indicated in the phase diagrams of figure 1 and exemplified in the panels (d_j) of figure 2, as well as in the column identified by (c_j) of figure 3. Due to the immiscibility, rotating droplet-like density peaks are formed near to the surface of the BEC in the first component; being located near the middle of the condensate for the second component.

For the row of panels with the densities given in the first and third rows of figure 3, we show the corresponding phases in the second and fourth rows of the same figure. These plots with the phases feature the corresponding vorticity, such that we can see the vorticity corresponding to the droplets in the column with (c_j). In the structure of the droplets that are being shown for the phases, we observe about vorticity two in the small-size droplets, and about four in the large-size droplets. These structures are similar to the double-core structures, where droplets in any one of the components are formed by multiple vortices with the same circulation, with vortices in any of those components being surrounded by those multiple vortices.

For the same ^{164}Dy-^{162}Dy mixture, in figure 4 we are verifying the vortex-pattern structure when increasing the rotation parameter, from the 0.5 that was used in figures 2 and 3 to $\Omega = 0.9$. By comparing both the cases given by figures 2 and 4 in the regime with $\delta > 1.45$, we noticed that rotating droplets are no longer supported and we particularly observed the formations of domain walls in the binary mixture. As the rotation becomes stronger, the binary mixture expands in the plane, being distributed in a larger radius. In this regime with $\delta > 1$, the droplet density peaks change to domain walls due to the large number of vortices, which become connected with

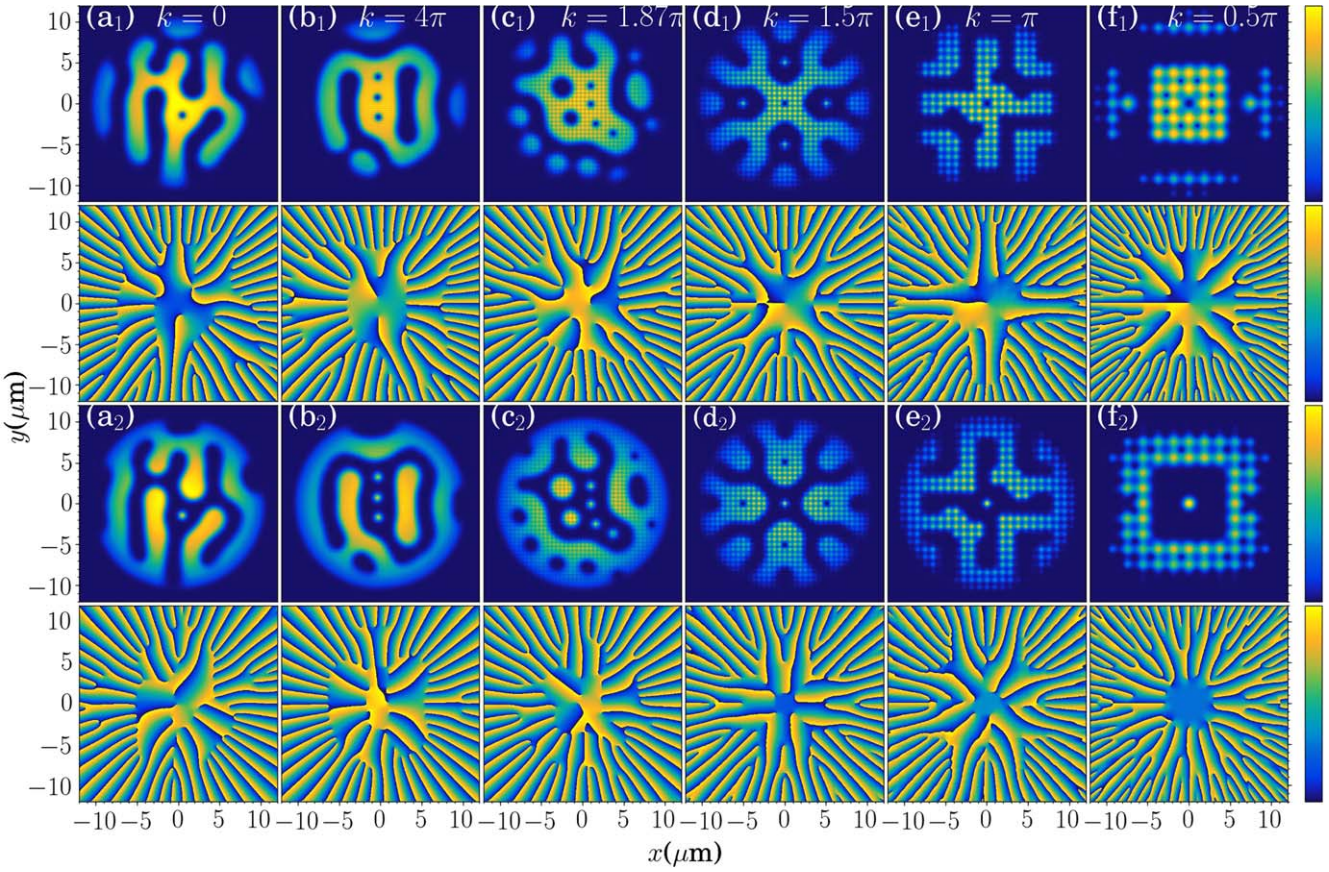

Figure 3. The effect of the OL in the vortex-lattice patterns shown in figure 2 is verified by an array of panels where the densities are given in the 1st and 3rd rows ($j = 1, 2$, respectively), followed by the corresponding phases, in the 2nd and 4th rows. For that, we fix $\delta = 1.45$ and vary the OL parameter k (OL is switched off for $k = 0$), keeping all the other parameters as in figure 2. As shown, the OL potential has stronger impact in the patterns in the interval $0.5\pi \lesssim k \lesssim 2\pi$. The mapping levels are from zero (darker) to 0.012 (clearer) for the densities and from $-\pi$ to π for the phases.

each other. However, as we decrease δ below one, we return to vortex-lattice structures having square formats.

3.2.3. ^{164}Dy-^{162}Dy mixture, with attractive DDI. The orientation of the dipoles is expected to be relevant, considering that by changing the both aligned dipoles from $\varphi = 0°$ to $\varphi = 60°$ we are also changing the strength of the DDI from a repulsive to an attractive one. Therefore, with the objective of verifying how much the vortex-lattice patterns could be affected by changing the orientation of the dipoles in this symmetric case, we present in figure 5 results corresponding to the ones we have verified in figures 2 to 4. Now, we consider the polarization of the dipoles making an angle $\varphi = 60°$ in relation to the orientation of the z-axis, such that the DDI becomes attractive. In order to compare with previous results, in figure 5 we consider the same rotation frequency $\Omega = 0.9$ as in figure 4. Again, we consider three values of the inter- to intra-species scattering lengths, given by δ (smaller, equal and larger than one). The main changes that we observe by comparing figures 4 and 5 are that the attraction in the DDI reduces the radius from ∼14 to ∼6 and, due to the increasing miscibility between the components, the patterns observed for $\delta > 1$ are somewhat similar to the ones verified in figures 2 and 3, with domain walls and with some rotating droplet formations (more restricted in this case due to more attraction between the components).

3.3. Asymmetric-dipolar mixture ^{168}Er-^{164}Dy in a squared OL

In this part of our study, we consider a condensed system with the asymmetric-dipolar coupled species ^{168}Er-^{164}Dy, which are confined in a pancake-shaped trap ($\lambda = 50$), with the addition of a squared OL. The parameters of the DDI in this case are given by $a_{11}^{(d)} = 66\, a_0$, $a_{22}^{(d)} = 131\, a_0$ and $a_{12}^{(d)} = a_{21}^{(d)} = 94\, a_0$. The main characteristics of this system in the absence of OLs is that the two components are less miscible, as studied before in [36]. The diagrams presented in figure 6 summarize the results we have obtained for the kind of vortex patterns that are found, considering the rotation of the system, given by the parameter Ω, and the inter- to intra-species contact interaction, δ. In diagram (A), we have considered the orientation of the two dipoles parallel to z, with $\varphi = 0$, implying a repulsive DDI. For the diagram (B), the orientation of the dipoles makes an angle $\varphi = 60°$ with respect to z, such that we have an attractive DDI.

As shown in diagram (A), the vortex patterns in the case of repulsive DDI are mainly with triangle shapes for $\delta \leqslant 0.9$ when we assume $\Omega \lesssim 0.8$, changing to squared shapes for larger Ω. And, for $\delta > 0.9$ the patterns are mainly circular

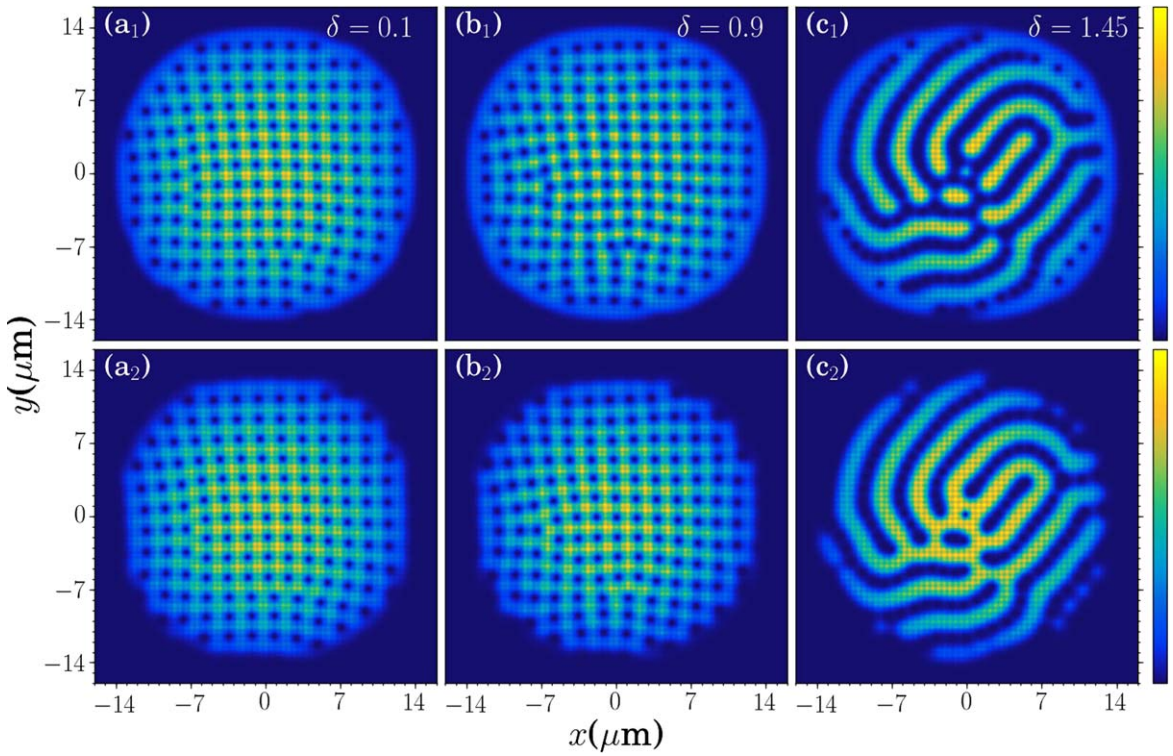

Figure 4. Effect of increasing the rotation frequency to $\Omega = 0.9$ in the densities shown in figure 2, where the DDI is repulsive ($\varphi = 0$). For the components $j = 1$ (upper) and 2 (lower), the panels are for $\delta = 0.1$, 0.9 and 1.45 (indicated inside the upper panels). The patterns have squared formats in (a_j) and (b_j), with striped and domain wall structures in (c_j). Other parameters and units are as in figure 2. Starting from zero (darker), the maximum density levels (clearer) are 0.005 4 for the panels (a_j) and (b_j), and 0.006 8 for the panels (c_j).

lattices, independently of the values of Ω. Patterns with rotating droplets are observed only for larger values of δ, close to $\sim$1.5 with Ω close to 0.9. In diagram (B), we have results considering attractive DDI, with $\varphi = 60°$. By comparing with diagram (A), we noticed that the triangle patterns remain only for smaller values of δ, as most of the results shown with $\delta < 1$ have squared pattern formats. Also, for $\delta > 1$, the attractive DDI increases the region where we can have patterns with droplets, which can happen when $\Omega \sim 0.9$. Sample results are given in the following three figures.

3.3.1. ^{168}*Er-*^{164}*Dy mixture, with repulsive DDI.* The results presented in figure 7 are for the densities of the two components, considering three values of δ, which give the ratio between inter- to intra-species scattering lengths. In this case, we are using the dipole orientations parallel to the z-axis ($\varphi = 0$), such that we have repulsive DDI. The rotation frequency is fixed to $\Omega = 0.5$. Due to the characteristics of this coupled system, we observe that in general we have circular patterns for the densities, where the less massive species (^{164}Dy, in this case) is distributed in a radius larger than the other one (^{168}Er). The repulsive DDI enhances the separation between the coupled species, in particular for larger values of δ (when the inter-species contact interaction is dominating). The vortex patterns are mostly triangular for $\delta < 1$ and with circular ring shapes for $\delta \geqslant 1$. The ^{168}Er-^{164}Dy mixture in a squared OL shows a triangular lattice within the regime where $\delta \leqslant 0.9$ and $\Omega < 0.85$. This coupled mixture, in the absence of an OL, presents a square vortex lattice for $\delta > 0.9$. The presence of the OL shows different vortex phase regimes. The circular shaped lattices are formed due to the complete phase separation of the condensates when $\delta > 0.9$, without being affected by the values of the rotation parameter Ω.

With the results presented in figure 8, we verify how the results given in figure 7 are affected by increasing the rotation. Therefore, we increase to 0.9 the value of Ω (in figure 7 is 0.5). As one can notice, by increasing the rotation the coupled system becomes more miscible, such that for $\delta > 1$ the circular patterns are not well defined as in figure 7 (see, for example, figure 11 of [21]). We can also verify the increasing number of rotating droplets and density peaks, which are formed due to multiple vorticity, as also discussed in the case of figure 3 for the ^{164}Dy-^{162}Dy mixture.

3.3.2. ^{168}*Er-*^{164}*Dy mixture, with attractive DDI.* Next, in figure 9, we change the orientation of the dipoles from $\varphi = 0$ (used in figure 8) to $\varphi = 60°$, such that the DDI becomes attractive. The effect of more attraction, and also by keeping the rotation high with $\Omega = 0.9$, is that the radius is reduced, as well as the number of vortices, with different vortex patterns being observed.

3.4. ^{164}*Dy-*^{52}*Cr and* ^{164}*Dy-*^{87}*Rb dipolar mixtures in a squared OL*

In this subsection we consider the coupled mixtures which have a stronger asymmetry, given by ^{164}Dy-^{52}Cr and

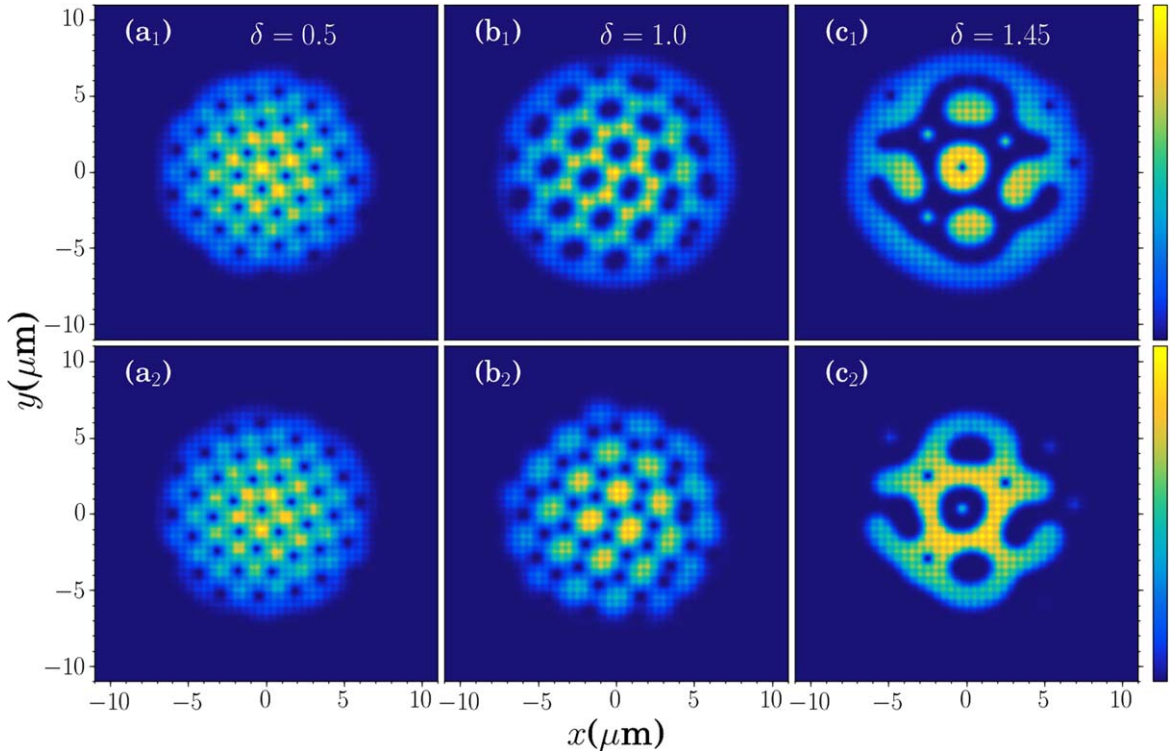

Figure 5. By keeping $\Omega = 0.9$, as in figure 4, we show the effect of changing the dipole orientations to an attractive DDI with $\varphi = 60°$. The panels are for $\delta = 0.5$, 1.0, and 1.45 (as indicated inside the upper panels), with other parameters as in figure 4. By comparing with figure 4, we noticed the vortex-lattice patterns change from squared formats to other geometric formats in (a_j) and (b_j) (going to hexagon-like formats) and from striped to domain walls with rotating droplets in (c_j). Starting from zero (darker), the maximum density levels (clearer) are 0.021 in all the panels.

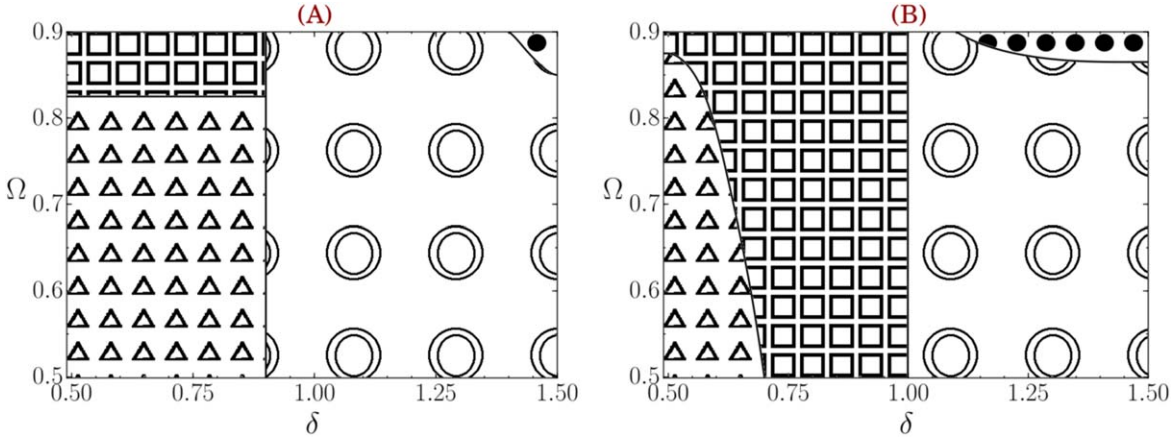

Figure 6. Diagrammatical representations of observed vortex-lattice patterns for the asymmetric ^{168}Er-^{164}Dy dipolar mixture, with the rotation frequency Ω as function of the contact interaction ratio $\delta \equiv a_{12}/a_{11}$. Both dipoles are polarized: along the z-axis ($\varphi = 0$) in (A); and at an angle $\varphi = 60°$ in (B). The symbols filling specific intervals indicate the approximate observed vortex-lattice patterns in these regions: triangles for triangular shaped, squares for squared shaped, concentric circles for circular lattices, and solid circles for 2D rotating droplets.

^{164}Dy-^{87}Rb. Besides their dipole properties, these systems have also a larger mass difference than the ones considered before. In these cases, considering the dysprosium as the first component, the corresponding parameters of the DDI are $a_{11}^{(d)} = 131\, a_0$, $a_{22}^{(d)} = 16\, a_0$ and $a_{12}^{(d)} = a_{21}^{(d)} = 25\, a_0$ for ^{164}Dy-^{52}Cr; with $a_{22}^{(d)}$ and $a_{12}^{(d)}$ almost zero for ^{164}Dy-^{87}Rb. We choose to give more details on the mixture with chromium, as in this case we have large asymmetry but with all non-zero dipolar parameters. The vortex-pattern results are shown through figures 10, 11 and 12, in analogy with the previous cases. With figure 13, we conclude this section with the corresponding vortex-pattern results for the densities obtained for the ^{164}Dy-^{87}Rb mixture, in which just one of the intra-species dipolar parameters is non-zero.

In each of the figures we display a set of three panels, considering three characteristic values of the parameter δ, for fixed rotations and dipole orientations. We start in figure 10, by considering $\Omega = 0.5$ and $\varphi = 0$ (repulsive DDI). As

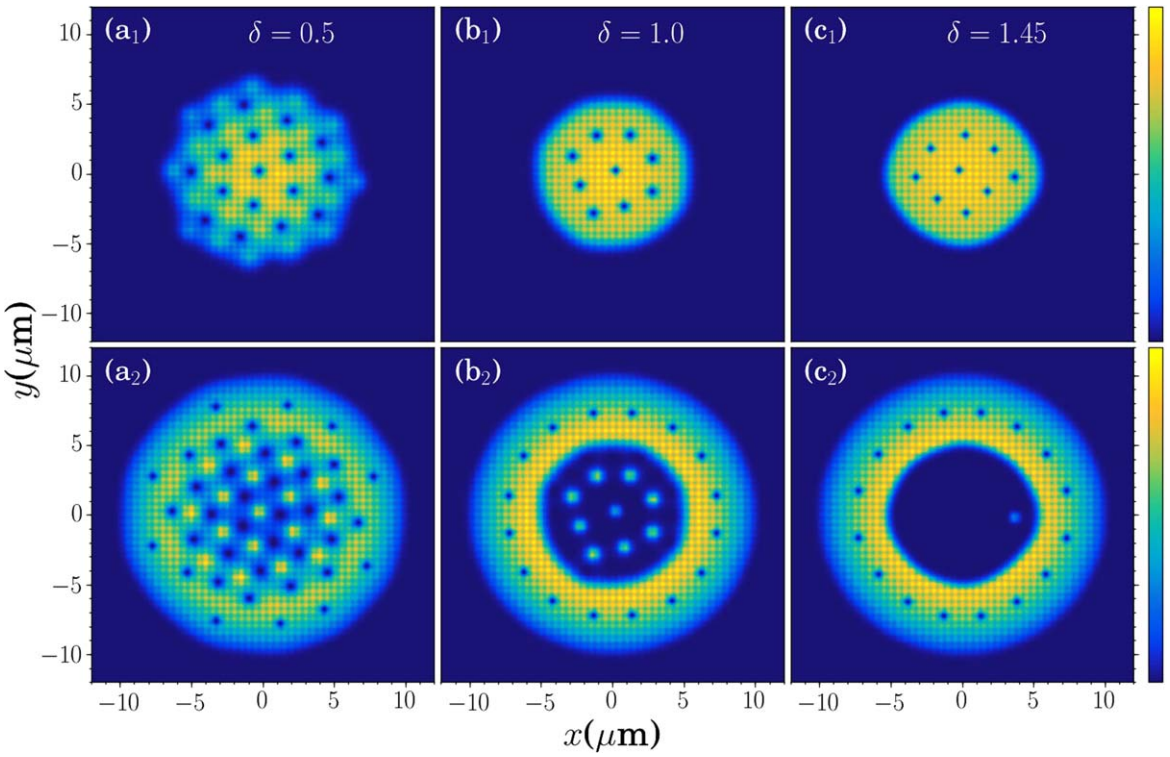

Figure 7. 2D densities of stable vortices for the dipolar mixture ^{168}Er-^{164}Dy (when $a_{11}^{(d)} = 66\ a_0$, $a_{22}^{(d)} = 131\ a_0$ and $a_{12}^{(d)} = a_{21}^{(d)} = 94\ a_0$) are shown in three sets of panels, for $\delta = 0.5$, 1.0 and 1.45 (as indicated inside the upper panels). The dipole orientations are parallel to z ($\varphi = 0$, repulsive DDI), with the rotation parameter $\Omega = 0.5$ (units ω_1). The OL parameters are $V_0 = 15$ (units $\hbar\omega_1$) and $\pi/k = 0.534$ (units μm). Starting from zero (darker), the maximum density levels are 0.014 for (a_1); 0.016 for (b_1) and (c_1); and 0.007 for the panels in the 2nd row.

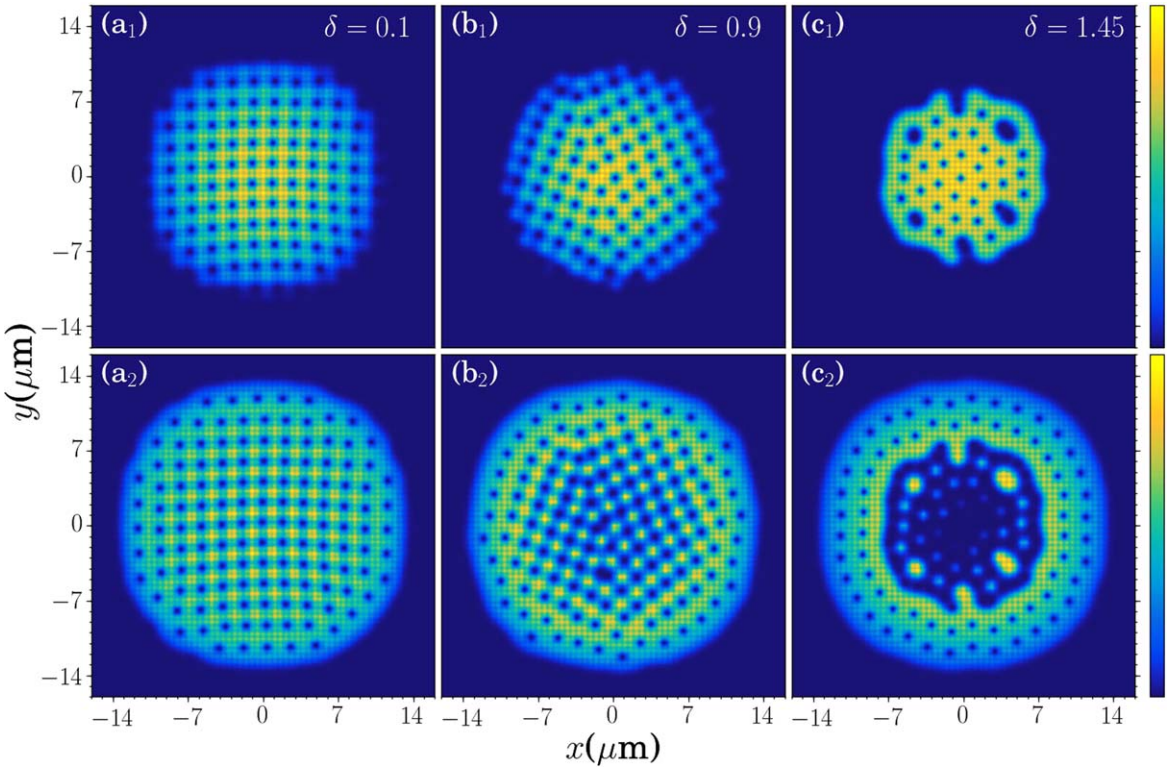

Figure 8. Effect of increasing the rotation frequency with $\Omega = 0.9$ in the density patterns shown in figure 7 for the ^{168}Er-^{164}Dy mixture, by considering the contact-ratio $\delta = 0.1$, 0.9 and 1.45 (as indicated inside the upper panels). Other parameters are the same as in figure 7. Starting from zero (darker), the maximum density levels are 0.007 3 for (a_1) and (b_1); 0.009 0 for (c_1); 0.004 5 for (a_2) and (b_2); and 0.005 8 for (c_2).

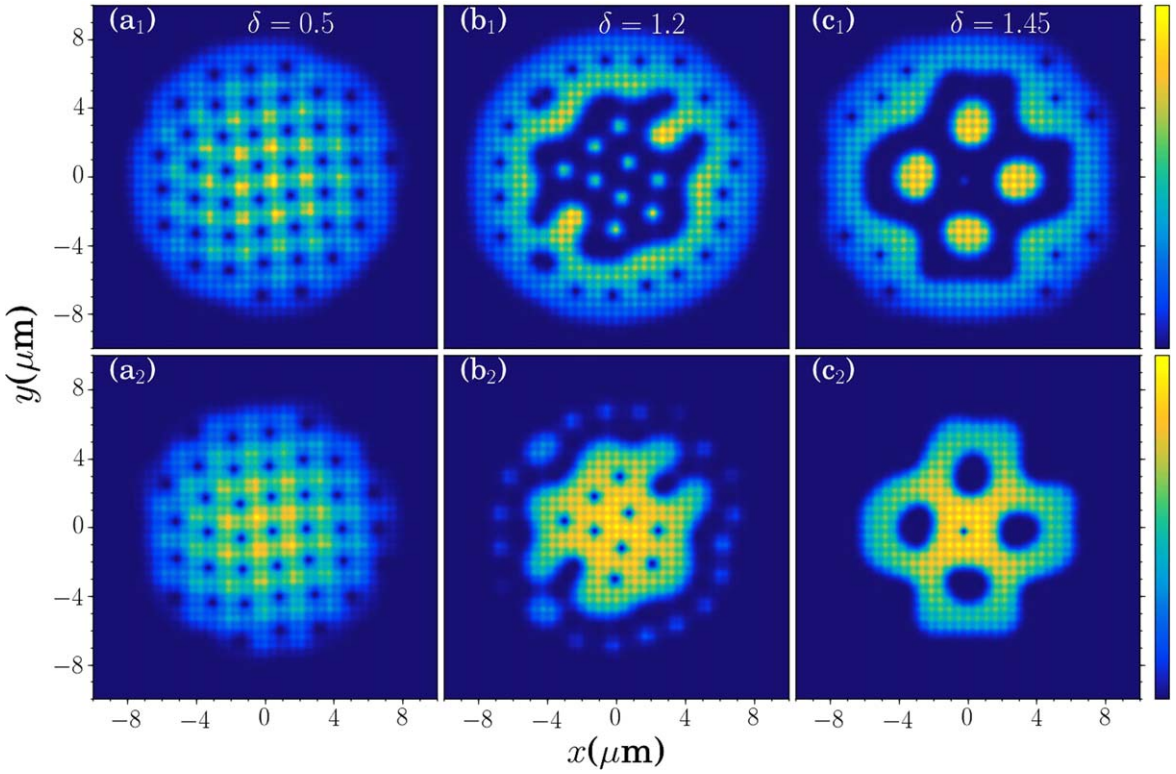

Figure 9. 2D density patterns are shown for the coupled mixture ^{168}Er-^{164}Dy in three sets of panels, with δ from 0.5, 1.2 and 1.45 (as indicated inside the upper frames), considering $\Omega = 0.9$ (as in figure 8) and the dipole orientations tuned to $\varphi = 60^{\circ}$ (attractive DDI). Other parameters are as in figures 7 and 8. The density levels are from zero to 0.019 for (a_1); 0.018 for (b_1); and 0.020 for the other panels.

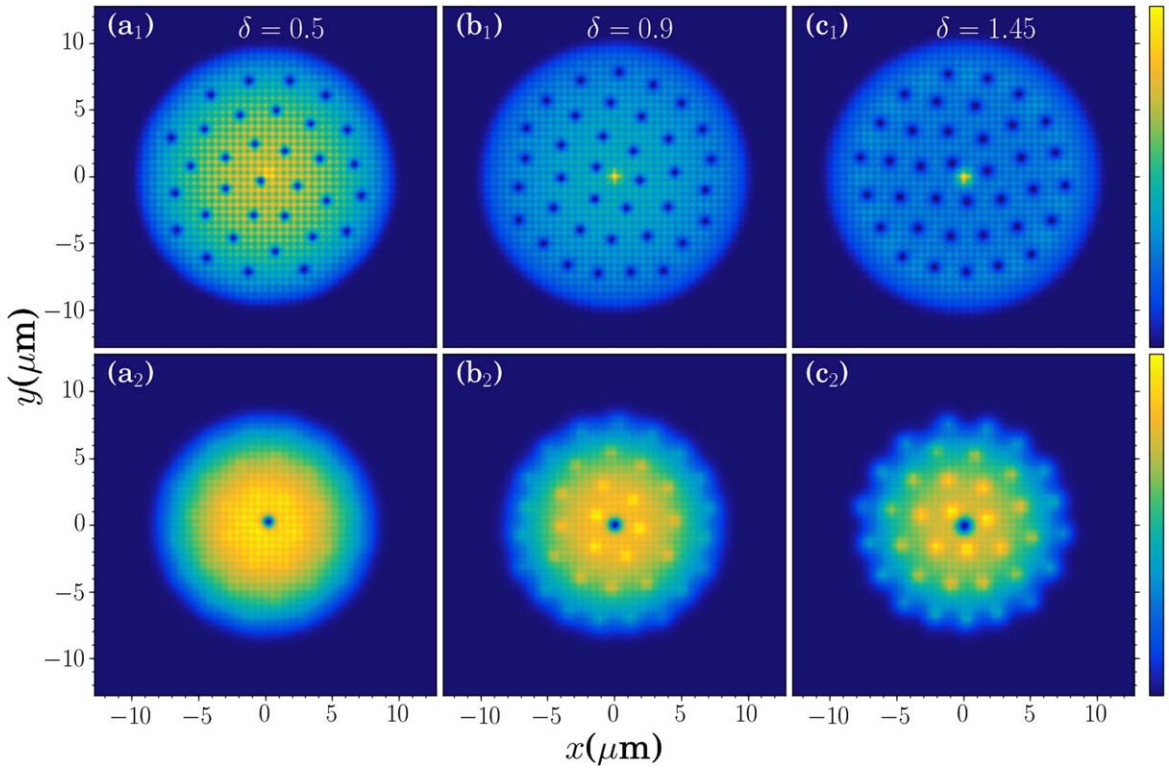

Figure 10. 2D densities $|\psi_{j=1,\,2}|^2$ of stable vortices for the dipolar mixture ^{164}Dy-^{52}Cr (when $a_{11}^{(d)} = 131\,a_0$, $a_{22}^{(d)} = 16\,a_0$ and $a_{12}^{(d)} = a_{21}^{(d)} = 25\,a_0$) are shown for $\delta = 0.5$, 0.9 and 1.45 (as indicated inside the upper frames), with $\Omega = 0.5$ and for repulsive DDI with $\varphi = 0^{\circ}$. The OL and other parameters are as in figure 7. The density levels are from zero to 0.010 for (a_1); 0.011 for (b_1); 0.013 for (c_1); and 0.009 for the other panels.

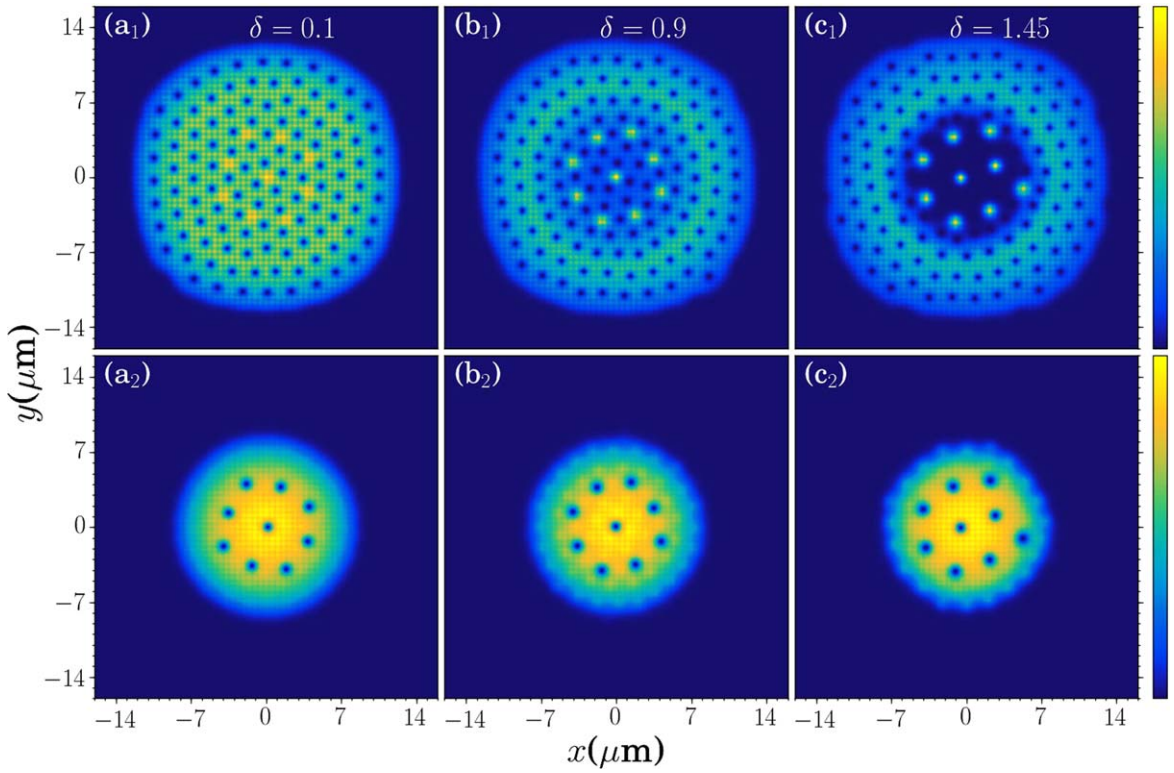

Figure 11. Effect of changing the rotation frequency to $\Omega = 0.9$ in the density patterns as given in figure 10, for the ^{164}Dy-^{52}Cr dipolar mixture with $\varphi = 0°$ (other parameters are as in figure 10). Starting with zero (darker), the maximum density levels are 0.013 0 for (a_1); 0.006 4 for (b_1); 0.007 8 for (c_1); 0.008 0 for (a_2) and (b_2); and 0.009 0 for (c_2).

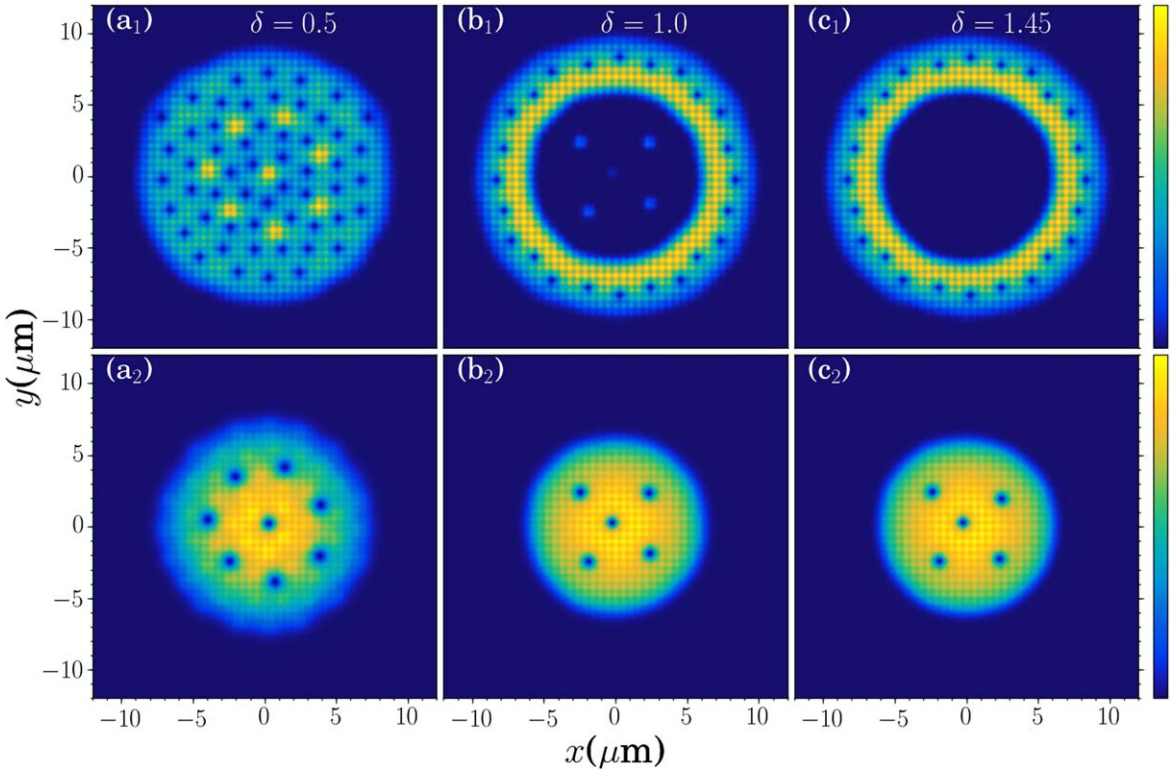

Figure 12. The 2D component densities of the mixture ^{164}Dy-^{52}Cr are shown with the same parameters as in figure 10, but with $\Omega = 0.9$ and $\varphi = 60°$ (attractive DDI). Starting from zero (darker), the maximum density levels are 0.011 for the 1st row and 0.012 for the 2nd row of panels.

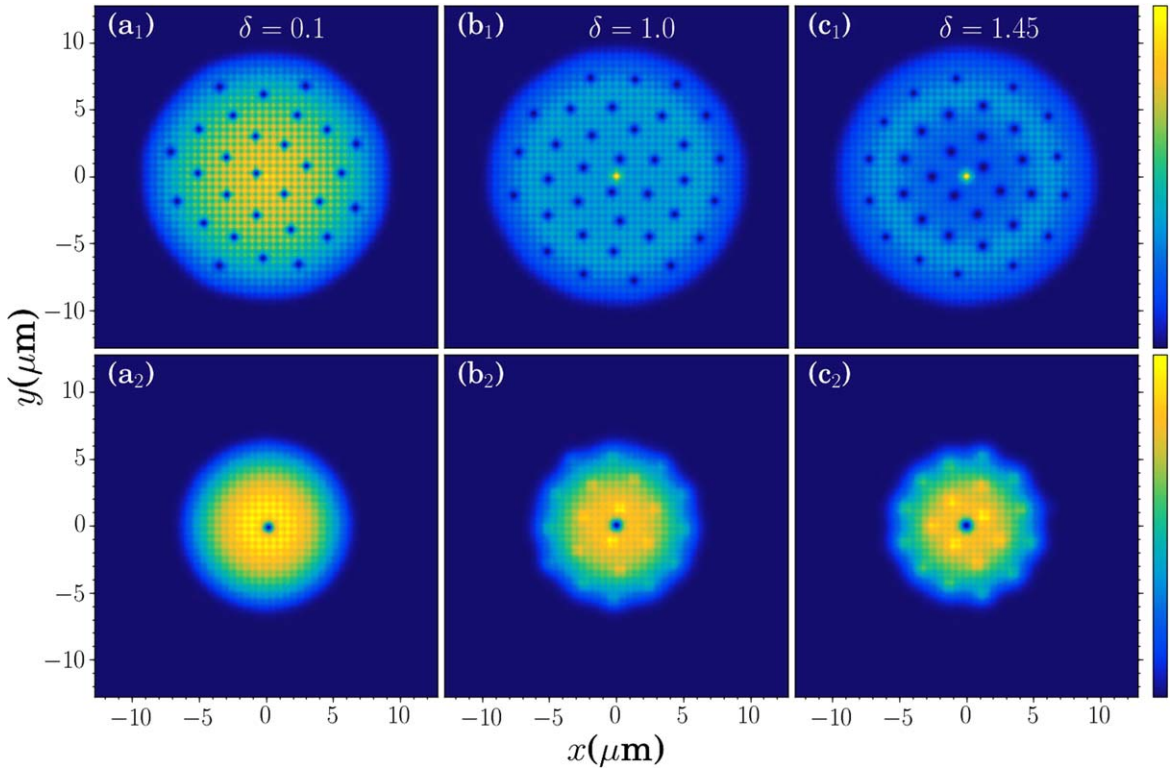

Figure 13. The 2D densities of stable vortices for the dipolar mixture ^{164}Dy-^{87}Rb (when $a_{11}^{(d)} = 131\, a_0$, with $a_{22}^{(d)}$ and $a_{12}^{(d)}$ negligible) are shown for $\delta = 0.1$, 1.0 and 1.45 (as indicated inside the upper frames), with $\Omega = 0.5$, and considering repulsive DDI ($\varphi = 0°$). The other parameters are as in figure 11. Starting from zero (darker), the maximum density levels are 0.010 for the 1st row and 0.009 for the 2nd row of panels.

verified, the density and number of vortices are distributed in a larger radius higher than 10 for the first component, the dysprosium, with the chromium density distributed in a smaller radius. In this case, this distribution of the density (in a larger space for the more massive species) is related to the repulsive intra-species dipolar interaction for the first component, $a_{11}^{(d)} = 131\, a_0$, which is about eight times larger than the intra-species interaction of the second component, $a_{22}^{(d)} = 16\, a_0$; and about five times larger than the inter-species interaction, $a_{12}^{(d)} = 25\, a_0$. As is also shown in this figure, the number of vortices in the second component is more affected by the changes in the inter- to intra-species parameter, increasing for $\delta > 1$.

Next, in figure 11, we increase the rotation parameter to $\Omega = 0.9$, keeping the same orientation of the dipoles parallel to z (repulsive DDI). As expected the radial distribution of the densities increases, in particular for the first component, where we also notice an increase in the number of vortices. The maximum localization of the distribution of this first component moves outside the center as the inter-species contact interaction is increased. For the second component, which has the density distributed closer to the center, we notice that an increasing rotation has the effect of increasing the number of vortices, which is clear for smaller values of δ. However, by increasing δ, with such $\Omega = 0.9$, the vortices merge together, as seen in the three panels.

With figure 12, we show the effect in the vortex patterns obtained for the ^{164}Dy-^{52}Cr dipolar mixture, by changing the DDI to an attractive one, with $\varphi = 60°$. In this case, we keep the same rotation parameter as in figure 11. By changing the DDI to attractive, the two densities become more concentrated, with almost all the density corresponding to the first component distributed in a ring around the 2nd component.

Finally, we present sample results of the densities for stable vortex-lattice distributions considering the ^{164}Dy-^{87}Rb dipolar mixture, in the three panels of the figure 13. As this case is similar to the case where we have chromium instead of rubidium, with larger asymmetry in the dipolar properties of the two species, we consider a case where the other parameters (except the dipolar ones) are the same as the ones considered in figure 10, with a repulsive DDI ($\varphi = 0$) and rotation given by $\Omega = 0.5$. As in the other cases, δ varies from 0.5 to 1.45.

The net difference between the two cases in this comparison is the decrease in the vorticity. The comparison between the results obtained for coupled dipolar mixtures with one of the species having a strong dipole strength, the ^{164}Dy, with two cases where the second components have weak or zero dipole strengths, such as ^{52}Cr and ^{87}Rb, is quite indicative of the behavior of mixtures when we have a non-dipolar component.

4. Summary and conclusions

In our study of structural vortex-lattice transitions with binary mixtures of dipolar BECs trapped in a strong pancake-type symmetry and loaded in a rotating squared OL, we consider the following mixtures of dipolar isotopes: ^{164}Dy-^{162}Dy, ^{168}Er-^{164}Dy, ^{164}Dy-^{52}Cr and ^{164}Dy-^{87}Rb. As the strength of the corresponding dipolar interactions are fixed for these systems, we consider two possible orientations of both aligned dipoles, by tuning the polarization angle to $\varphi = 0$ or 60° with respect to the z-axis. By using these two orientations, we consider repulsive DDIs ($\varphi = 0$), as well as attractive ones ($\varphi = 60^{\circ}$). Once the intrinsic dipolar properties of the binary mixture have been considered, together with the trap conditions (pancake-type with aspect ratio $\lambda = 50$) and OL parameters, the other main physical variables in our study to produce different lattice-vortex patterns are the ratio between inter- to intra-species two-body interaction δ and the rotation frequency Ω (in units of the trap frequency ω_1).

By considering the kind of patterns which are obtained in our numerical investigation, for different pairs of parameters Ω and δ, all the results for the symmetric ^{164}Dy-^{162}Dy and asymmetric ^{168}Er-^{164}Dy dipolar mixtures are summarized in two diagrams given in figures 1 and 6, respectively. The diagrams are followed by specific examples of vortex-pattern results. For the other binary mixtures, we just choose representative results of the vortex-lattice structures. In the specific results, which are being displayed along this work, we consider two representative values for the rotation parameter, $\Omega = 0.5$ and 0.9, corresponding to low- and high-rotation speed. For the squared OL, the strength is fixed to $V_0 = 15$ with a lattice grid given by $\pi/k = 0.534$ (units of μm), suggested by existing experimental possibilities. The lattice parameter k was varied in the specific case of the symmetric-dipolar mixture, showing a way to control the vortex-lattice patterns and indicating the grid interval where the OL potential is dominant. Besides that, the vortex-lattice structures are changed by varying the inter-species contact interactions, with the assumption that the corresponding intra-species interactions are kept equal for both species.

The symmetric ^{164}Dy-^{162}Dy dipolar mixture was first analyzed—as it is more appropriate to verify the OL effect—in both the cases that we have a repulsive or attractive DDI, by tuning the dipole orientations φ. As compared with studies having no OL potential, we noticed that the addition of a squared OL potential (in the plane defined by the pancake-type trap) has the effect of changing triangle vortex-lattice patterns to squared formats when $\delta \lesssim 1$. However, for $\delta \geqslant 1$, a structural transition in the patterns is observed, with the OL reinforcing patterns with stripes, with domain walls and vortex sheets. In particular, interesting 2D rotating droplet vortex structures are observed by increasing the asymmetry between inter- and intra-species interaction (such as we have exemplified, with $\delta \sim 1.45$). A relatively shallow OL facilitates the appearance of droplet vortex structures in some particular regimes of the parameters δ and Ω. For the strength of the OL we select $V_0 = 15$, after verifying that the vortex-lattice structures are in general similar. We have also observed that droplets lattice patterns are not supported with a deeper OL such as with $V_0 > 25$, when considering rotation frequency is not high, near $\Omega = 0.5$. As the frequency is increased, with $\Omega > 0.65$, more vortices are established, which start to connect together forming domain-wall structures, with droplet vortex patterns no longer being verified.

We change the DDI strength from a repulsive (when $\varphi = 0$) to an attractive one, by tuning the dipole orientation to $\varphi = 60^{\circ}$. In this case, anisotropic effects due to the dipolar interaction are visualized with the radius of the condensed mixture being significantly reduced in relation to the case that $\varphi = 0$ (see figures 4 and 5). When the DDI becomes attractive, we also note that the effect of the OL is less pronounced. The attractive two-body interactions, either by contact or DDI, reduce the number of vortices, with the phase diagram becoming similar to the case of dipolar mixtures in harmonic traps. The main different characteristic is that the OLs support rotating droplet vortex structures for $\delta > 1.3$ and $\Omega > 0.875$. As the interactions are attractive, the number of vortices is not enough to create droplets for $\Omega < 0.875$. In the regime with $\delta > 1.3$ and $\Omega < 0.875$, we have only separated phase mixtures with few vortices.

Next, we study the asymmetric-dipolar mixture ^{168}Er-^{164}Dy, which is verified to be less miscible in previous studies where there are no OL interactions. Again we consider two phase diagrams in a plane defined by Ω and δ, given in figure 6, for summing up our results for the lattice-vortex patterns. As verified in such a case, there is no relevant effect verified in the vortex-lattice patterns by varying the rotation frequency Ω, which are mainly squared-vortex lattices for $\delta < 1$, with a circular vortex lattice for $\delta > 1$. On the other hand, after applying the squared OL on this asymmetric mixture, we can verify that the vortex-lattice patterns are more affected by changing the rotation frequency. As indicated in the $\delta - \Omega$ phase diagram presented in the left frame of figure 6, for the case that the polarized dipoles are aligned with the z-axis ($\varphi = 0$), when $\delta < 0.9$, the vortex-lattice patterns produced are mainly with triangular formats when $\Omega < 0.85$, changing to squared formats when $\Omega > 0.85$. For $\delta > 0.9$ the vortex-lattice structures are predominantly with concentric circles, with rotating droplet vortex-lattice patterns being verified in the limited regime for large values of δ ($\sim$1.45) and Ω ($\sim$0.9). Sample illustrative vortex-lattice patterns are shown in figure 9. Further, by changing the DDI to be attractive, with $\varphi = 60^{\circ}$, as shown in the right frame of the figure 6, for $0.7 < \delta < 1$, most of the patterns change from triangular (when the DDIs are repulsive) to squared formats (when the DDIs are repulsive), except for smaller values of δ where the triangular formats remain. Droplet vortex structures can also be observed in the high-rotation regime, where Ω is close to 0.9, when $\delta > 1.2$. See, for example, the patterns (c_i) shown in figure 8, in this case.

More briefly we consider the highly asymmetric mixtures, with larger differences in the mass and dipole moments, as ^{164}Dy-^{52}Cr and ^{164}Dy-^{87}Rb. These mixtures show only triangular and half-quantum vortex lattices. The dipole moment of ^{164}Dy is comparatively much larger than the dipole moments of the other component. So, the first

component (^{164}Dy) produces more vortices than the second one. Besides that, we have observed that both ^{164}Dy-^{52}Cr and ^{164}Dy-^{87}Rb present similar characteristics.

In our present investigation, we have studied dipolar-symmetric and dipolar-asymmetric binary systems, which are confined in stable pancake-shaped configurations with fixed OL parameters, where most of the results are shown for two moderate low and high-rotation frequencies ($\Omega = 0.5$ and 0.9). Apart from that, for the vortex-pattern structures, the inter- to intra-species repulsive contact interactions δ and the polarization angle of the DDI φ are the main relevant parameters to be considered. The miscibility of the two components is reduced by increasing δ, provides the different domain-wall shaped vortex structure in the dipolar-symmetric case; and in radial space separations of the components in the dipolar-asymmetric case. The polarization angle can change the system from repulsive to attractive, by going to larger angles, which will reduce the radius, having relevant effects on the pattern structures, particularly for larger δ, in the interplay between repulsive contact interactions (increasing the immiscibility) and the attractive DDI (reducing the radial distribution of the densities).

The OL parameters are adjusted when considering possible experimental setups, so as to not strongly affect the behavior of other relevant quantities we are studying. A specific example is presented in figure 3, where we show how the OL can affect the vortex-lattice patterns by changing the OL grid-spacing parameter. As observed, for values of k near zero (very large grid spacing), there are almost no oscillations along the trap, with practically no OL effect. Also, in the other limit, for large values of k (very small grid spacing), the trap is practically not affected, because the oscillations will average to a constant. However, for intermediate values of k, we can have dramatic changes of patterns with further loss of cylindrical symmetry due to the alignment of the lattice and corresponding BEC localization.

Finally, we understand that the present results can be useful to calibrate on-going experiments with dipolar mixtures, such as the recent ones, ^{164}Dy-^{162}Dy and ^{168}Er-^{164}Dy, which are under active investigation, when considering pancake-type trap symmetries and loaded in-squared OLs.

Acknowledgments

We thank the Brazilian agencies FAPESP—Fundação de Amparo à Pesquisa do Estado de São Paulo (Procs. 2014/01668-8, 2016/17612-7 and 2017/05660-0), CNPq—Conselho Nacional de Desenvolvimento Científico e Tecnológico (Procs. 306191/2014-8 and 304468/2014-2) and CAPES—Coordenação de Aperfeiçoamento de Pessoal de Nível Superior (LT), for partial financial support.

ORCID iDs

Ramavarmaraja Kishor Kumar https://orcid.org/0000-0003-2898-2002

Lauro Tomio https://orcid.org/0000-0002-2811-9797

References

[1] Bloch I, Dalibard J and Zwerger W 2008 *Rev. Mod. Phys.* **80** 885
[2] Greiner M, Mandel O, Esslinger T, Hänsch T W and Bloch I 2002 *Nature* **415** 39
[3] Fisher M P A, Weichman P B, Grinstein G and Fisher D S 1989 *Phys. Rev.* B **40** 546
[4] Greiner M, Bloch I, Mandel M O, Hänsch T and Esslinger T 2001 *Phys. Rev. Lett.* **87** 160405
[5] Öttl A, Ritter S, Köhl M and Esslinger T 2005 *Phys. Rev. Lett.* **95** 090404
[6] Bakr W S, Peng A, Tai M E, Ma R, Simon J, Gillen J I, Fölling S, Pollet L and Greiner M 2010 *Science* **329** 547
[7] Myatt C J, Burt E A, Ghrist R W, Cornell E A and Wieman C E 1997 *Phys. Rev. Lett.* **78** 586
[8] Ferrier-Barbut I, Kadau H, Schmitt M, Wenzel M and Pfau T 2016 *Phys. Rev. Lett.* **116** 215301
[9] Schmitt M, Wenzel M, Böttcher F, Ferrier-Barbut I and Pfau T 2016 *Nature* **539** 259
[10] Chomaz L, Baier S, Petter D, Mark M J, Wächtler F, Santos L and Ferlaino F 2016 *Phys. Rev.* X **6** 041039
[11] Ferrier-Barbut I, Wenzel M, Böttcher F, Langen T, Isoard M, Stringari S and Pfau T 2018 *Phys. Rev. Lett.* **120** 160402
[12] Chomaz L, van Bijnen R M W, Petter D, Faraoni G, Baier S, Becher J H, Mark M J, Wächtler F, Santos L and Ferlaino F 2018 *Nature Phys.* **14** 442
[13] Ilzhöfer P, Durastante G, Patscheider A, Trautmann A, Mark M J and Ferlaino F 2018 *Phys. Rev.* A **97** 023633
[14] Trautmann A, Ilzhöfer P, Durastante G, Politi C, Sohmen M, Mark M J and Ferlaino F 2018 *Phys. Rev. Lett.* **121** 213601
[15] Müller S, Billy J, Henn E, H Kadau H, Griesmaier A, Jona-Lasinio M, Santos L and Pfau T 2011 *Phy. Rev.* A **84** 053601
Billy J, Henn E A L, Müller S, Maier T, Kadau H, Griesmaier A, Jona-Lasinio M, Santos L and Pfau T 2012 *Phys. Rev.* A **86** 051603(R)
[16] Lahaye T, Menotti C, Santos L, Lewenstein M and Pfau T 2009 *Rep. Prog. Phys.* **72** 126401
[17] Baranov M A, Dalmonte M, Pupillo G and Zoller P 2012 *Chem. Rev.* **112** 5012
[18] Tung S, Schweikhard V and Cornell E A 2006 *Phys. Rev. Lett.* **97** 240402
[19] Williams R A, Al-Assam S and Foot C J 2010 *Phys. Rev. Lett.* **104** 050404
[20] Kasamatsu K, Tsubota M and Ueda M 2003 *Phys. Rev. Lett.* **91** 150406
[21] Kumar R K, Tomio L, Malomed B A and Gammal A 2017 *Phys. Rev.* A **96** 063624
[22] Reijnders J W and Duine R A 2004 *Phys. Rev. Lett.* **93** 060401
Reijnders J W and Duine R A 2005 *Phys. Rev.* A **71** 063607
[23] Pu H, Baksmaty L O, Yi S and Bigelow N P 2005 *Phys. Rev. Lett.* **94** 190401
[24] Kasamatsu K and Tsubota M 2006 *Phys. Rev. Lett.* **97** 240404
[25] Martin A M, Marchant N G, O'Dell D H J and Parker N G 2017 *J. Phys.: Condens. Matter* **29** 103004
[26] Yi S and Pu H 2006 *Phys. Rev.* A **73** 061602(R)
[27] Malet F, Kristensen T, Reimann S M and Kavoulakis G M 2011 *Phys. Rev.* A **83** 033628
[28] Kumar R K and Muruganandam P 2012 *J. Phys. B: At. Mol. Opt. Phys.* **45** 215301
Kumar R K and Muruganandam P 2014 *Eur. Phys. J.* D **68** 289
Kumar R K, Sriraman T, Fabrelli H, Muruganandam P and Gammal A 2016 *J. Phys. B: At. Mol. Opt. Phys.* **49** 155301
[29] Xi K-T, Byrnes T and Saito H 2018 *Phys. Rev. A* **97** 023625

[30] Zhang X-F, Han W, Jiang H-F, Liu W-M, Saito H and Zhang S-G 2016 *Ann. of Phys.* **375** 368
Wang L-X, Dong B, Chen G-P, Han W, Zhang S-G, Shi Y-R and Zhang X-F 2016 *Phys. Lett.* A **380** 435
[31] Inouye S *et al* 1998 *Nature* **392** 151
[32] Zeng R and Zhang Y 2009 *Comp. Phys. Commun.* **180** 854
[33] Ao P and Chui S T 1998 *Phys. Rev.* A **58** 4836
[34] Wen L, Liu W M, Cai Y, Zhang J M and Hu J 2012 *Phys. Rev.* A **85** 043602
[35] Pattinson R W, Billam T P, Gardiner S A, McCarron D J, Cho H W, Cornish S L, Parker N G and Proukakis N P 2013 *Phys. Rev.* A **87** 013625
Pattinson R W 2014 Two-component Bose–Einstein condensates: equilibria and dynamics at zero temperature and beyond *PhD Thesis* Newcastle University, Newcastle, UK
[36] Kumar R K, Muruganandam P, Tomio L and Gammal A 2017 *J. Phys. Commun.* **1** 035012
[37] Lu M, Burdick N Q, Youn S H and Lev B L 2011 *Phys. Rev. Lett.* **107** 190401
[38] Tang Y, Kao W, Li K and Lev B L 2018 *Phys. Rev. Lett.* **120** 230401
[39] Góral K and Santos L 2002 *Phys. Rev.* A **66** 023613
[40] Giovanazzi S, Görlitz A and Pfau T 2002 *Phys. Rev. Lett.* **89** 130401
[41] Salasnich L 2002 *Laser Phys.* **12** 198
Salasnich L, Parola A and Reatto L 2002 *Phys. Rev.* A **65** 043614
[42] Salasnich L and Malomed B A 2009 *Phys. Rev.* A **79** 053620
[43] Kumar R K, Young-S L E, Vudragović D, Balaž A, Muruganandam P and Adhikari S K 2015 *Comput. Phys. Commun.* **195** 117
[44] Wilson R M, Ticknor C, Bohn J L and Timmermans E 2012 *Phys. Rev.* A **86** 033606
[45] Ticknor C, Wilson R M and Bohn J L 2011 *Phys. Rev. Lett.* **106** 065301
[46] Müller S, Billy J, Henn E A L, Kadau H, Griesmaier A, Jona-Lasinio M, Santos L and Pfau T 2011 *Phys. Rev.* A **84** 053601
[47] Gammal A, Frederico T and Tomio L 2001 *Phys. Rev.* A **64** 055602
Gammal A, Tomio L and Frederico T 2002 *Phys. Rev.* A **66** 043619
Brtka M, Gammal A and Tomio L 2006 *Phys. Lett.* A **359** 339
[48] Muruganandam P and Adhikari S K 2009 *Comp. Phys. Commun.* **180** 1888
Vudragović D, Vidanović I, Balaž A, Muruganandam P and Adhikari S K 2012 *Comp. Phys. Commun.* **183** 2021
[49] Butts D A and Rokhsar D S 1998 *Nature* **397** 327
[50] Bao W, Wang H and Markowich P A 2005 *Comm. Math. Sci.* **3** 57
[51] Jeng B W, Wang Y S and Chien C S 2013 *Comput. Phys. Commun.* **184** 493
[52] Kasamatsu K, Tsubota M and Ueda M 2005 *Int. J. Mod.* **19** 1835
[53] Saarikoski H, Reimann S M, Harju A and Manninen M 2010 *Rev. Mod. Phys.* **82** 2785